Electronic Supplementary Information (ESI)

A hybrid superconcentrated electrolyte enables 2.5 V carbon-based supercapacitors

Weijian Wang[a], Wenjun Deng[a], Xusheng Wang[b], Yibo Li[a], Zhuqing Zhou[a],
Zongxiang Hu[a], Mianqi Xue[b] and Rui Li[a]*

[a] School of Advanced Materials, Peking University Shenzhen Graduate School, Shenzhen 518055, China.

[b] Technical Institute of Physics and Chemistry, Chinese Academy of Sciences, Beijing 100190, China.

*Corresponding author: liruisz@pku.edu.cn

Experimental

Preparation of hybrid superconcentrated (HSC) electrolyte: The HSC electrolyte was prepared by molality (mol-salt in kg solvent). In a typical synthesis, LiFSI (5.984 g) was dissolved into distilled water (1.00 g) to form a 32 m LiFSI-H_2O “water-in-salt” electrolyte, then LiFSI (4.114 g) was dissolved into organic solvent EC/DMC (volume ratio of 1:1, 2.00 g) to form an 11 m LiFSI-EC/DMC electrolyte, and the HSC electrolyte was obtained by mixing 32 m LiFSI in water and 11 m LiFSI in EC/DMC (vol. 1:1) at a mass ratio of 1:2, and it is equivalent to an apparent LiFSI concentration 14.6 m.

Electrolyte Characterizations: The ionic conductivities of the electrolytes were measured by using an electrical conductivity meter DDS-307 (INESA Scientific Instrument Co., Ltd.). Viscosity was measured by a rotational rheometer Haake MARS Ⅲ (Thermo Fisher Scientific, Germany). Electrochemical stability potential windows of electrolytes were determined by linear sweep voltammetry measurements using an electrochemical workstation (CHI660D) at a scan rate of 10 mV s^{-1} within -3.2 to 3.2 V *vs*. saturated calomel electrode (SCE). Raman spectra were measured using a Lab Ram HR Evolution Series High Resolution Raman Spectrometer

(HORIBA Jobin Yvon SAS, France). The thermal properties of the electrolytes were investigated by differential scanning calorimetry (Netzsch DSC METTLER TOLEDO DSC1) with a temperature range from 80 to -50 °C.

Preparation of the Electrodes: All the electrodes were made from 80 wt.% of commercial activated carbon (AC, YP-50, Kuraray Chemical, Japan), 10 wt.% of the binder (polytetrafluoroethylene, PTFE) and 10 wt.% of conductive material (Ketjen black). The electrode slices (7 mm diameter) were dried at 110 °C at a vacuum oven for 12 h, then were pressed onto the current collector (Ti mesh). Each electrode loading of AC is about 4 mg cm^{-2}.

Electrochemical Measurements: The symmetric AC//AC system was assembled in coin cell type CR2032 with two YP-50 electrodes and glass fibers were used as the separators. Cyclic voltammetry (CV) and Electrochemical Impedance Spectroscopy (EIS) tests were performed on an electrochemical workstation (CHI660D). Galvanostatic charge/discharge (GCD) tests were carried out by using a battery test system (NEWARE). The voltage recording of the cathode and anode during the charge/discharge process of the symmetric AC//AC system was carried out by a Solartron 1470E multi-channel potentiostats electrochemical workstation using a three-electrode system.

Electrodes Measurements: Scanning electron microscopy (SEM) image of the electrode surface after cycling was performed on a ZEISS SUPRA-55 scanning electron microscope. The surface element valence of the electrode surface after cycling was investigated by X-ray photoelectron spectra (XPS, Thermo Scientific, Escalab 250Xi).

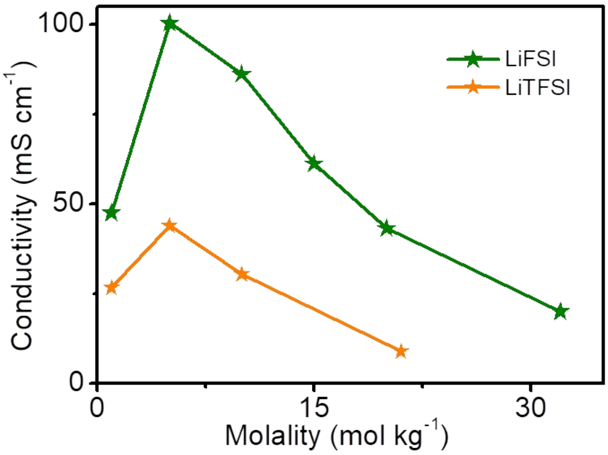

Fig. S1 Conductivity of the LiFSI and LiTFSI electrolytes with different concentrations at room temperature. The ionic conductivity can reach 100.3 mS cm^{-1} for 5 m LiFSI while the value is only 43.9 mS cm^{-1} for 5 m LiTFSI, and the conductivity of 32 m LiFSI is 19.9 mS cm^{-1}.

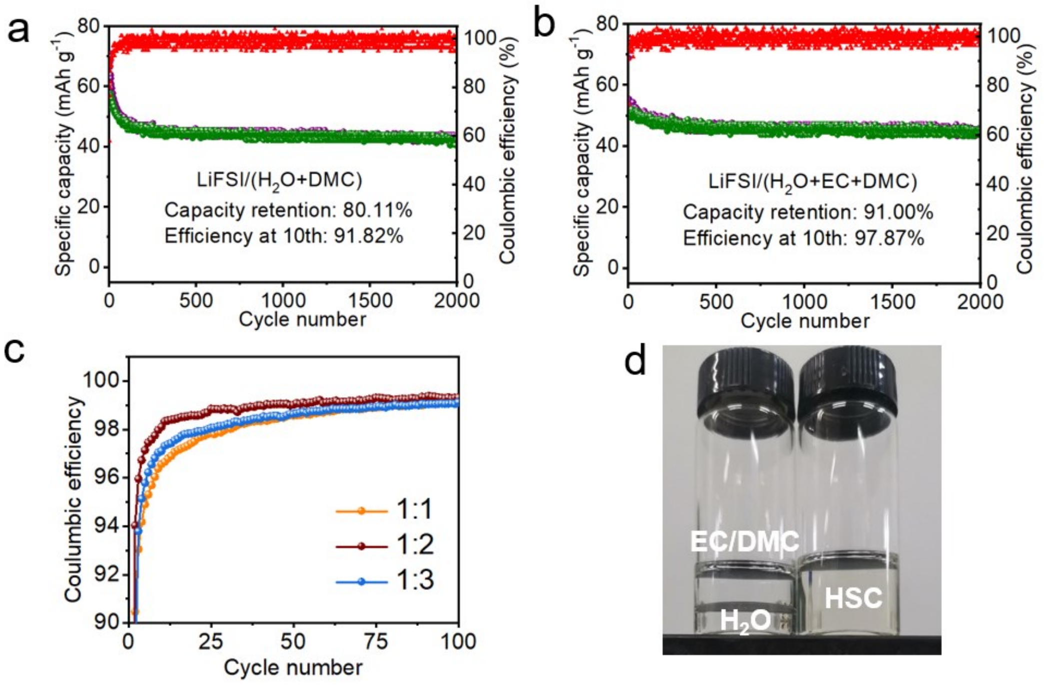

Fig. S2 Cycling performance and coulombic efficiency of the AC//AC supercapacitors using (a) 32 m LiFSI/H_2O + 11 m LiFSI/DMC and (b) 32 m LiFSI/H_2O + 11 m LiFSI/(DMC+EC) electrolytes with an operating voltage of 2.5 V at 1 A g^{-1}, and the supercapacitors using LiFSI/(H_2O+EC+DMC) electrolyte exhibit higher efficiency and better cycle stability than using LiFSI/(H_2O+DMC). (c) Efficiency performance at different mass ratios for 32 m LiFSI/H_2O:11 m LiFSI/(DMC+EC), and the highest charge and discharge efficiency was obtained for the 1:2 ratio, indicating the fewest side reactions during cycling. (d) Immiscibility between water and organic solvents (EC+DMC) and the homogeneous of the HSC electrolyte after adding LiTFSI.

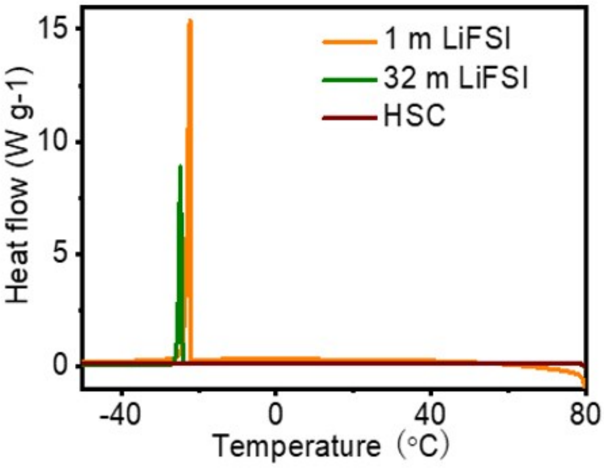

Fig. S3 Thermal properties of the three electrolytes within a temperature range from 80 to -50 °C at a cooling rate of 5 °C min^{-1}. The thermograms display the exothermic peaks around -22 °C and -25 °C for 1 m LiFSI and 32 m LiFSI, respectively, whereas completely flat in the case of HSC, which means that the HSC electrolyte is still in a liquid state even at -50 °C, while the 1 m LiFSI and 32m LiFSI solutions are frozen, indicating a wide operating temperature for HSC electrolyte.

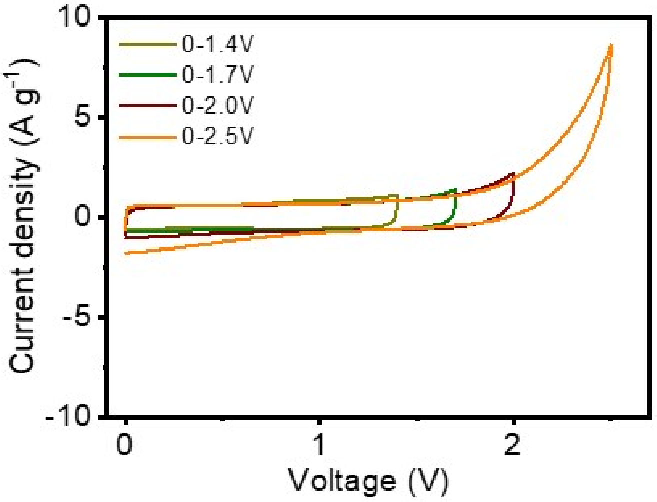

Fig. S4 CV curves of the AC//AC supercapacitors using the 1 m LiFSI electrolyte at different voltage range at a scan rate of 10 mV s^{-1}.

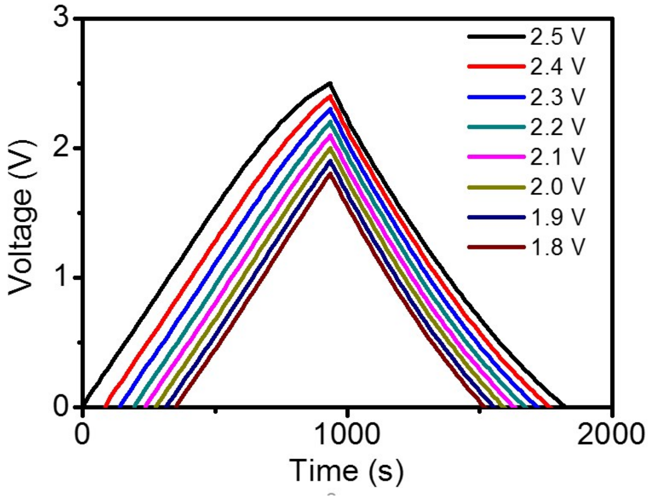

Fig. S5 Galvanostatic charge-discharge characteristics recorded for a symmetric AC//AC supercapacitor in HSC at different operating voltage from 1.8 to 2.5 V at a current density of 200 mA g^{-1}.

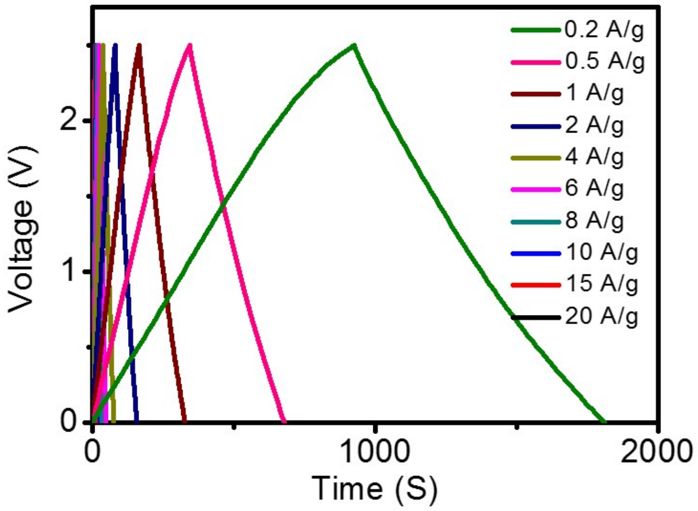

Fig. S6 Galvanostatic charge-discharge curves at various current densities from 0.2 to 20 A g^{-1} of the supercapacitors using HSC electrolyte.

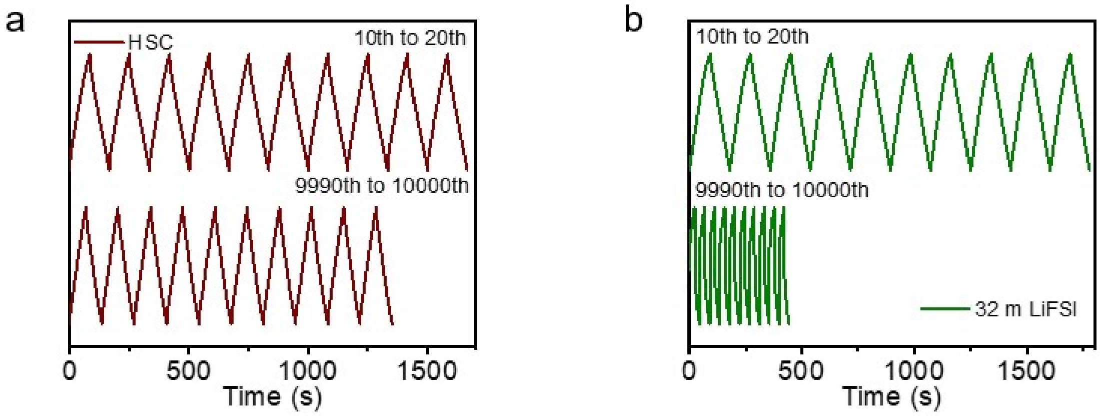

Fig. S7 Galvanostatic charge-discharge curves from 10th cycle to 20th cycle and from 9990th cycle to 10000th cycle of the AC//AC symmetric supercapacitor using HSC electrolyte which shows the discharge time retention of 82.1% (a), while the AC//AC symmetric supercapacitor using 32 m LiFSI electrolyte shows the discharge time retention of 24.93% (b), at a current density of 1 A g^{-1} at an operation voltage of 2.5 V.

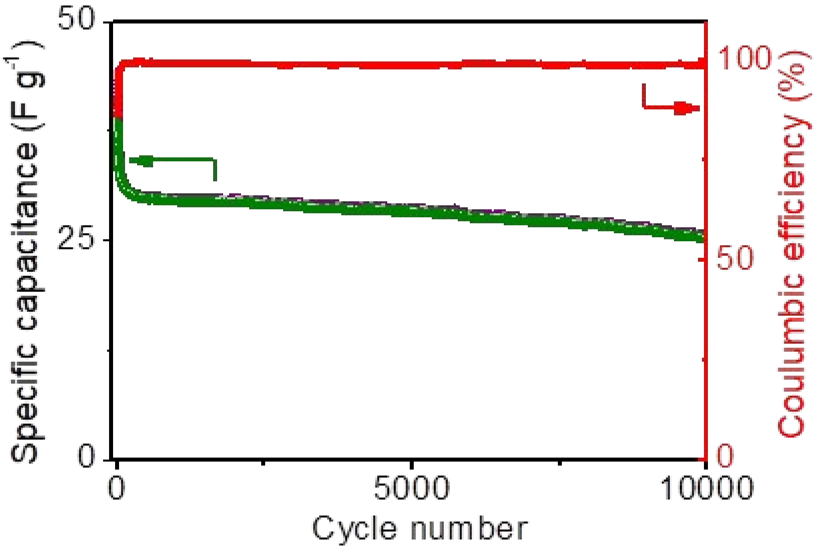

Fig. S8 Cycling performance and coulombic efficiency of the AC//AC symmetric supercapacitor using 1 m LiFSI electrolyte at an operation voltage of 2.0 V at a current density of 1 A g^{-1}.

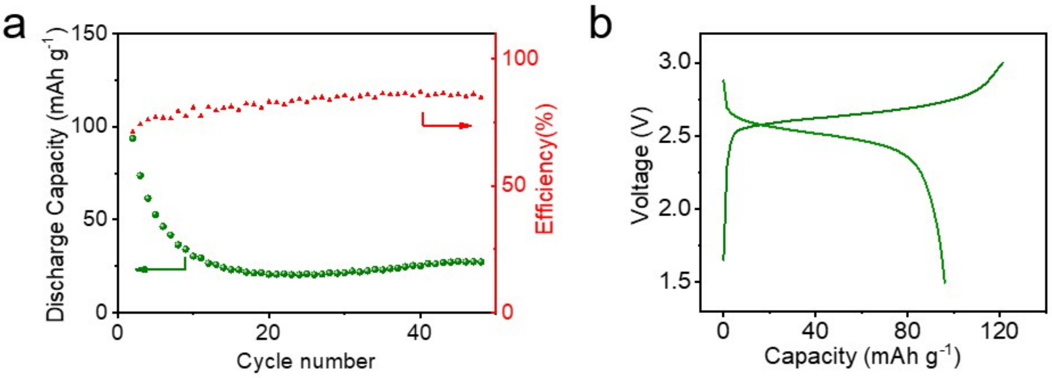

Fig. S9 (a) Cycling performance and coulombic efficiency of the $LiMn_2O_4/Li_4Ti_5O_{12}$ aqueous lithium-ion battery using HSC electrolyte at an operation voltage range from 1.5 V to 3.0 V at a current density of 0.15 A g^{-1}. (b) First cycle galvanostatic charge-discharge profiles of the $LiMn_2O_4/Li_4Ti_5O_{12}$ aqueous lithium-ion battery using HSC electrolyte at a current density of 0.15 A g^{-1}.

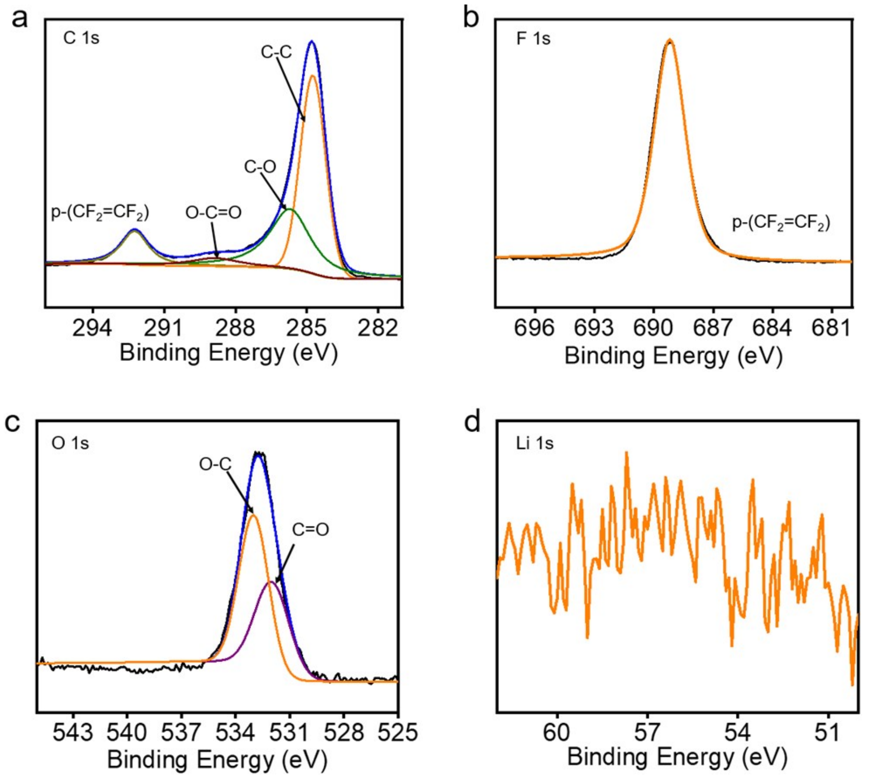

Fig. S10 XPS spectra for the electrode surface after cycling. (a) C 1s, (b) F 1s, (c) O 1s, (d) Li 1s.

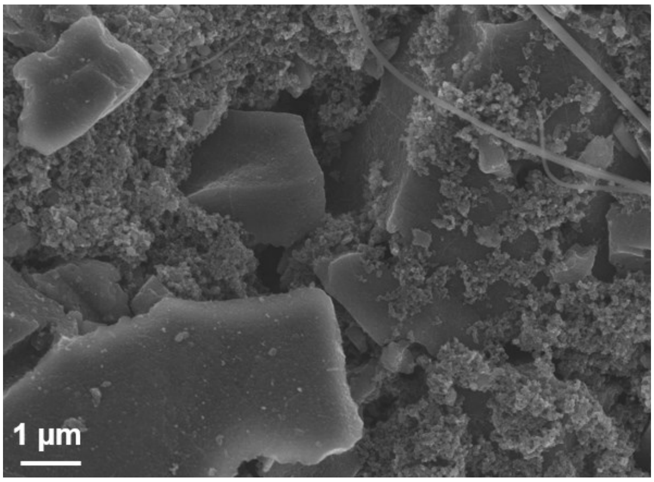

Fig. S11 SEM image for the electrode surface after cycling.

Table S1. The ionic conductivities and viscosities for the three electrolytes.

	1 m LiFSI	32 m LiFSI	HSC

Conductivity (mS cm^{-1})	47.43	19.92	3.78
Viscosity (mm^2 s^{-1})	22	66	373

Table S2. Comparison of the operating voltage and energy density versus recently published high-performance symmetric supercapacitors using aqueous concentrated electrolytes.

Carbon type	Operating voltage (V)	Electrolyte	Energy density (Wh kg^{-1})	Ref.
AC	2.0	75 wt% KAc	16.8	1
YP-50F	2.2	$LiTFSI(H_2O)_{2.6}(CH_3CN)_{3.7}$	Not mention	2
YP-50F	2.3	17 m $NaClO_4$	23.7	3
YP-50F	2.3	21 m LiTFSI	17.2	3
YP-50F	2.4	$LiTFSI/H_2O/(CAN)_{3.5}$	Not mention	4
3D high-density graphene	2.1	17 m NaClO4	22.3 Wh L^{-1}	5
YP-50F	**2.5**	**HSC**	**27.1**	**This work**

Table S3. Comparison of the average voltage versus recently published high-voltage lithium-ion batteries using aqueous concentrated electrolytes.

Cathode	Anode	Electrolyte	Average voltage (V)	Ref.
$LiMn_2O_4$	Mo_6S_8	21 m LiTFSI	2.3	6
$LiMn_2O_4$	TiO_2	21 m LiTFSI/7 m LiOTf	2.1	7
$LiCoO_2$	$Li4Ti_5O_{12}$	$Li(TFSI)_{0.7}(BETI)_{0.3}\cdot 2H_2O$	2.35	8
$LiNi_{0.5}Mn_{1.5}O_4$	$Li_4Ti_5O_{12}$	DMC/H_2O/LiTFSI (14 m)	3.2	9
$LiMn_2O_4$	**$Li_4Ti_5O_{12}$**	**HSC**	**2.5**	**This work**

Reference

1. Z. Tian, W. Deng, X. Wang, C. Liu, C. Li, J. Chen, M. Xue, R. Li and F. Pan, Funct. Mater. Lett., 2017, **10**, 1750081.
2. Q. Dou, S. Lei, D.-W. Wang, Q. Zhang, D. Xiao, H. Guo, A. Wang, H. Yang, Y. Li, S. Shi and X. Yan, Energy Environ. Sci., 2018, **11**, 3212-3219.
3. X. Bu, L. Su, Q. Dou, S. Lei and X. Yan, J. Mater. Chem. A, 2019, **7**, 7541-7547.
4. D. Xiao, Q. Dou, L. Zhang, Y. Ma, S. Shi, S. Lei, H. Yu and X. Yan, Adv. Funct. Mater., 2019, **29**, 1904136.
5. L. Zhang, D. Wu, Q. Ma, G. Wang, Z. Liu, M. Chang and X. Yan, ChemElectroChem, 2020, **7**, 838-845.
6. L. Suo, O. Borodin, T. Gao, M. Olguin, J. Ho, X. Fan, C. Luo, C. Wang and K. Xu, Science, 2015, **350**, 938-943.

7. L. Suo, O. Borodin, W. Sun, X. Fan, C. Yang, F. Wang, T. Gao, Z. Ma, M. Schroeder, A. von Cresce, S. M. Russell, M. Armand, A. Angell, K. Xu and C. Wang, Angew. Chem. Int. Ed., 2016, **55**, 7136-7141.
8. Y. Yamada, K. Usui, K. Sodeyama, S. Ko, Y. Tateyama and A. Yamada, Nat. Energy, 2016, **1**, 16129.
9. F. Wang, O. Borodin, M. S. Ding, M. Gobet, J. Vatamanu, X. Fan, T. Gao, N. Eidson, Y. Liang, W. Sun, S. Greenbaum, K. Xu and C. Wang, Joule, 2018, **2**, 927-937.